Glycine-Functionalized Copper(II) Hydroxide Nanoparticles with High Intrinsic Superoxide Dismutase Activity

K. Korschelt,[a] R. Ragg,[a] C. S. Metzger,[b] M. Kluenker,[a] M. Oster,[a] B. Barton,[a] M. Panthöfer,[a] D. Strand,[c] U. Kolb,[a] M. Mondeshki,[a] S. Strand,[c] J. Brieger,[b] M. N. Tahir[a*] & W. Tremel[a*]

[a] Institute of Inorganic and Analytical Chemistry, Johannes Gutenberg University Mainz, Duesbergweg 10-14, 55128 Mainz, Germany, Correspondence and requests for materials should be addressed to M.N.T. (*tahir@uni-mainz.de) and W.T. (*tremel@uni-mainz.de)

[b] Department of Otorhinolaryngology, Head and Neck Surgery, Laboratory of Molecular Tumor Biology, University Medical Center of the Johannes Gutenberg University, 55101 Mainz, Germany

[c] Department of Internal Medicine, University Medical Center, Johannes Gutenberg University Mainz, Obere Zahlbacher Straße 63, 55131 Mainz, Germany

Supporting information

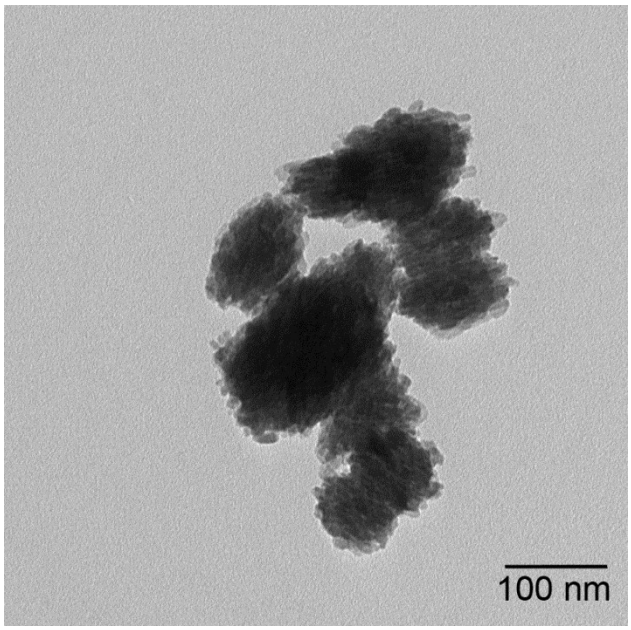

Fig. S1. TEM image of $Cu(OH)_2$ precipitated from an aqueous solution of copper(II) sulfate, glycine and of sodium hydroxide solution. The synthesis of Gly-$Cu(OH)_2$ NPs was not successful directly from the components without isolating the *cis*-bis(glycinato) copper(II) monohydrate ($Cu(Gly)_2$) intermediate. Only an insoluble $Cu(OH)_2$ precipitate was formed instead.

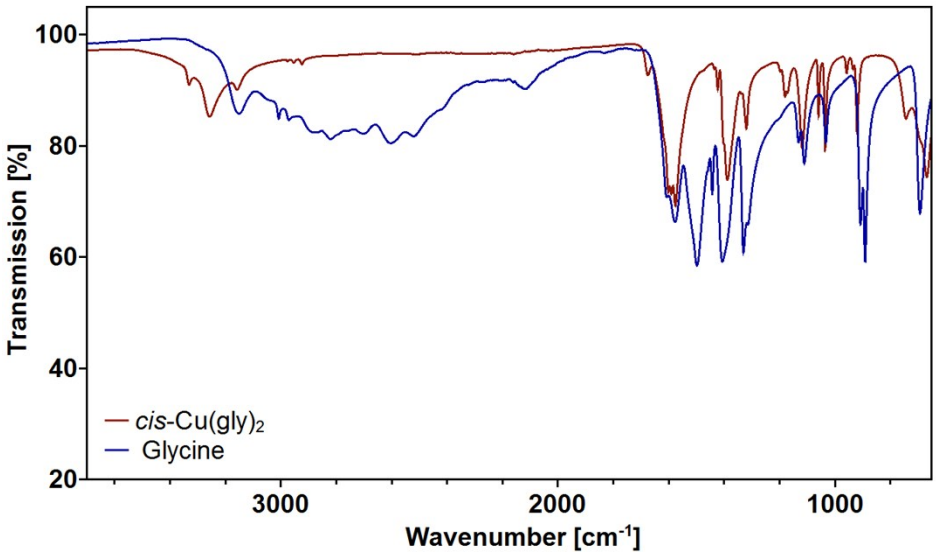

Fig. S2. IR spectra of *cis*-bis(glycinato) copper(II) monohydrate (red line) and glycine (blue line). Characteristic bands: NH_2 vibration[1,2] at 3331, 3254 and 3157 cm^{-1}; asym. COO stretch at 1603 cm^{-1} ; sym. COO stretch at 1386 cm^{-1}.[1,2]

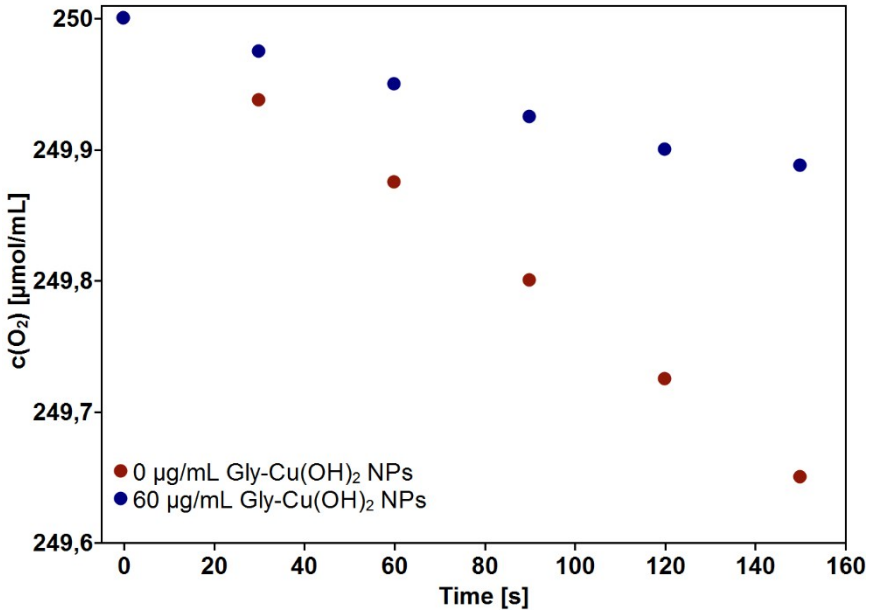

Fig. S3. Oxygen evolution of Gly-Cu(OH)$_2$ NPs when exposed to superoxide radicals generated by xanthine/xanthine oxidase (XO)**.** Molecular oxygen (O_2) is depleted by the enzymatic activity of XO (red) forming superoxide radicals. In general superoxide dismutation by SOD-active materials leads to the formation of hydrogen peroxide and oxygen (50% each). Gly-Cu(OH)$_2$ NPs reduce the oxygen depletion to approx. 50% (blue), which is equivalent to the formation of an equivalent amount of O_2.

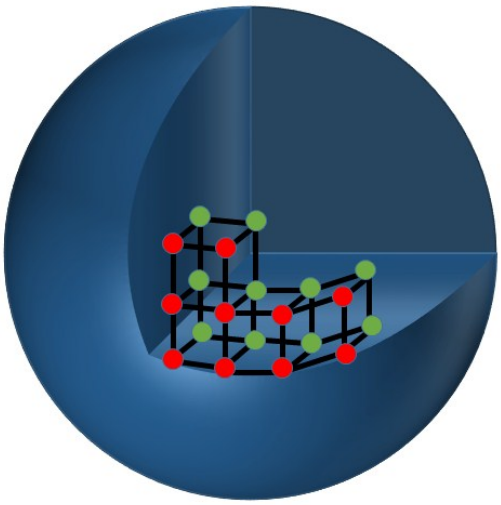

Fig. S4. Schematic representation of a spherical $Cu(OH)_2$ NP and showing the catalytically active Cu atoms at the NP surface (red) and inactive atoms inside the NP volume (green). To simplify the representation a simple cubic unit cell instead of the orthorhombic lepidocrocyte structure of $Cu(OH)_2$ is shown.

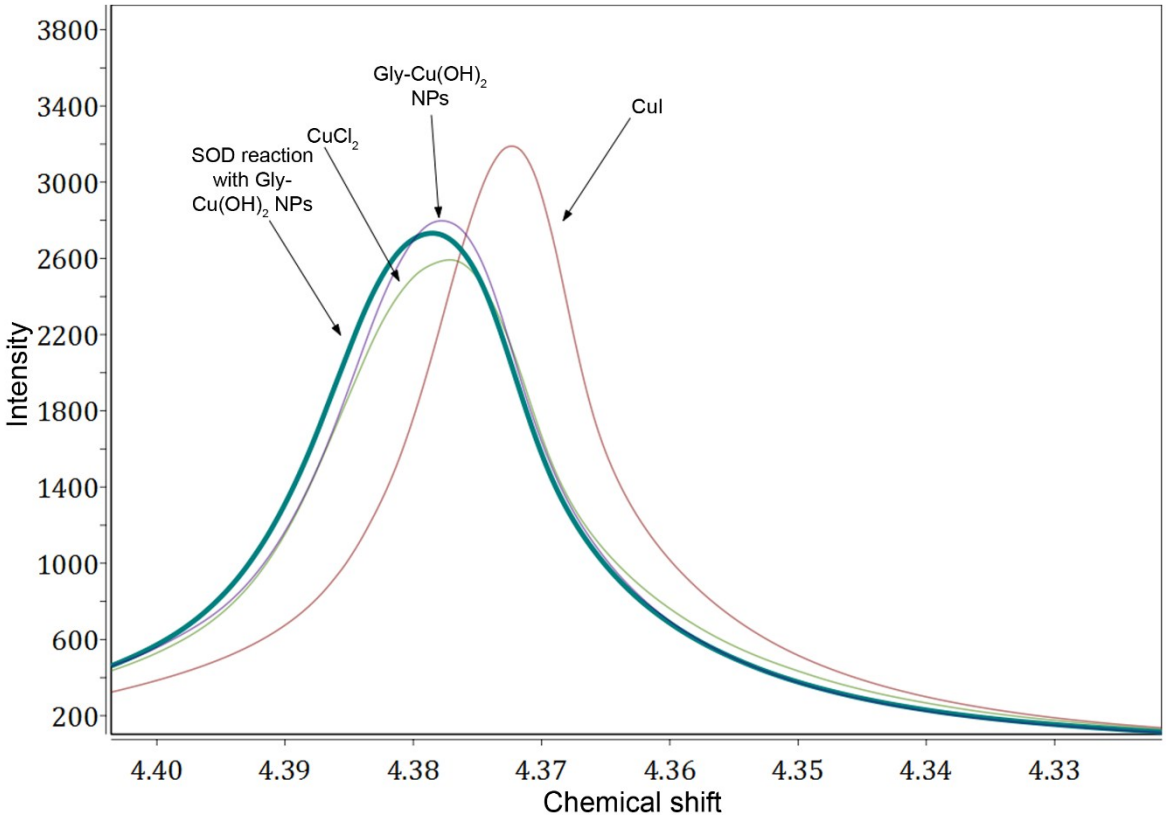

Fig. S5. NMR spectra of the SOD-like reaction catalyzed by Gly-Cu(OH)$_2$ NPs recorded with the Evans method.[3] The ^{1}H-NMR signal of an aqueous solution of paramagnetic copper(II) compounds (Gly-Cu(OH)$_2$ NPs and $CuCl_2$) shows a broadened and downfield shifted H_2O resonance with respect to a solution containing diamagnetic CuI. For the water signal after the SOD-like reaction a paramagnetic shift was observed, which can be explained with the shuttling of copper between the oxidation states +II and +I during the reaction and the recovery of the catalyst.

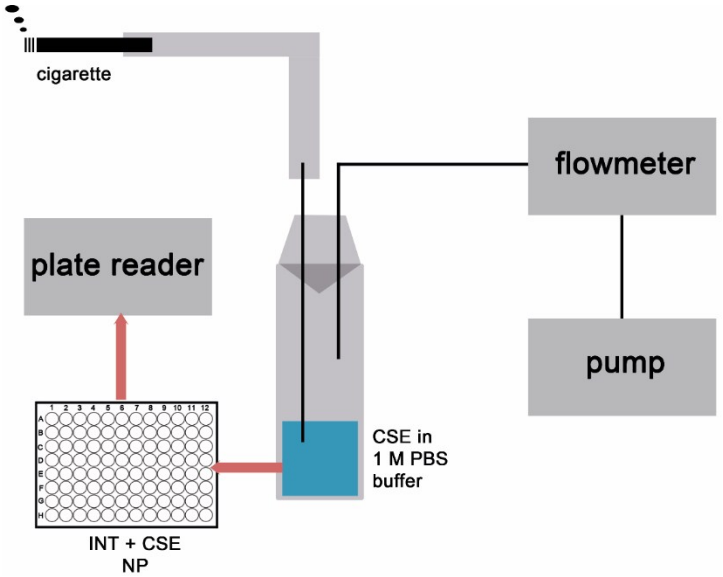

Fig. S6. Setup for cigarette smoke experiments. A cigarette smoke extract (CSE) was produced using a commercial Magnum cigarette. A constant maelstrom (0.3-0.5 $L \cdot min^{-1}$) was ensured with a vacuum pump and a flowmeter. The CSE extract was analyzed with INT as superoxide sensitive dye and different amounts of Gly-$Cu(OH)_2$ NPs on a 96-well-plate reader.

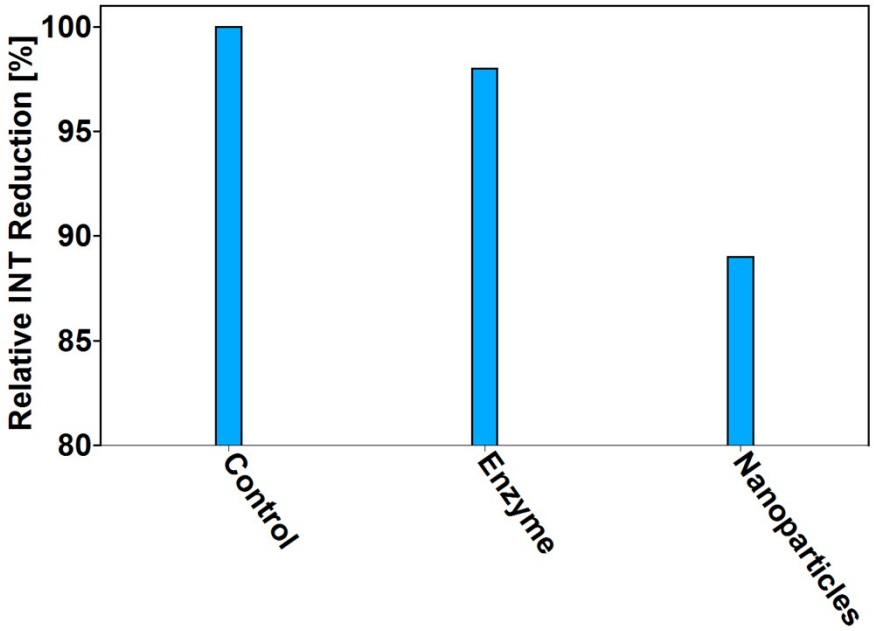

Fig. S7. Inhibition of INT reduction by Gly-Cu(OH)$_2$ NPs and CuZn SOD shows a higher efficiency of reducing superoxide level of the Gly-Cu(OH)$_2$ NPs.

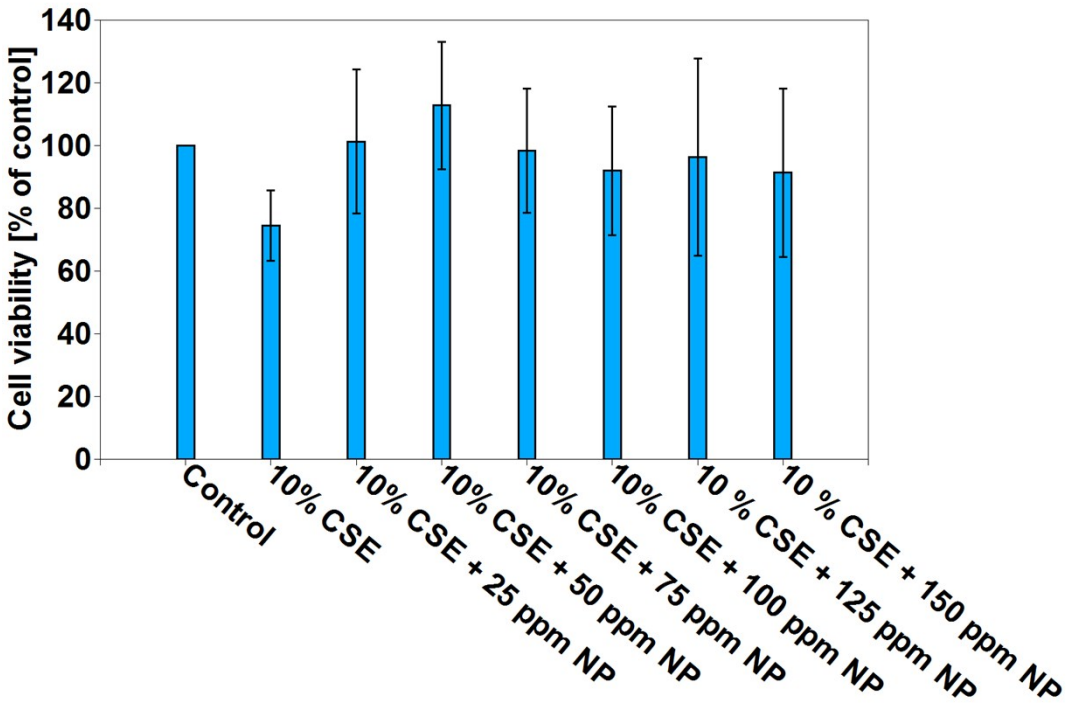

Fig. S8. Cytotoxicity of cigarette smoke extract (CSE) for A549 cells. The cytotoxicity was determined with an AlamarBlue® assay after reacting the cells with CSE that were treated before with different amounts of Gly-$Cu(OH)_2$ NPs.[4] A 10% CSE showed toxic behavior. Treating the CSE with Gly-$Cu(OH)_2$ NPs reduced the cytotoxicity.

Tab. S1. Details of the X-ray powder diffraction measurement and the refinement of the x-ray diffraction data.

	Gly-$Cu(OH)_2$ NPs
Diffractometer	Siemens D5000
Sample preparation	Powder between two Scotch ® Magic tape stripe
Measuring mode	Transmission
Wavelength	$CuK\alpha_1$, 1.540596 Å
Measuring range	$10 \leq 2\Theta\ /° \leq 90$, $\Delta 2\Theta/° = 0.0078$; $0.72 \leq Q/Å^{-1} \leq 5.76$
	2s /step, sum of 2 individual scans
Temperature / K	298
Profile fit	Rietveld refinement according to reported crystal structure models
Background / Parameters	Chebyshev / 16
Profile function	Fundamental Parameters Approach / correction for anisotropic crystallite size
Program	TOPAS Academic V5.0
No. of variables	25
R_{exp}	1.70
R_{wp}	1.31
GoF	1.45
Durban-Watson statistic	0.96
$Cu(OH)_2$	
Space group	$Cmc2_1$
Cell parameters /Å	a = 2.9474(7)
	b = 10.630(5)
	c = 5.305(2)
Crystallite size /nm	13.4(4) by 5.4(1) by 6.6(1)
Fraction /%wt	100
B_{iso}	1.0(1)

Tab. S2. Catalytic activities of Gly-$Cu(OH)_2$ NPs, bulk $Cu(OH)_2$ and natural CuZn SOD with respect to molar concentration and *per* active site.

sample	Concentration to receive a 50% inhibition of the INT reduction [$\mu g \cdot mL^{-1}$]	IC_{50} for molar NP concentrations [μM]	IC_{50} *per* active site [μM]	k for molar NP concentrations [$M^{-1}s^{-1}$]	k *per* active site [$M^{-1}s^{-1}$]
Gly-$Cu(OH)_2$ NPs	$0.101 \pm 2.0 \cdot 10^{-3}$	$2.25 \cdot 10^{-14}$	$5.02 \cdot 10^{-10}$	$8.72 \cdot 10^{14}$	$3.91 \cdot 10^{10}$
CuZn SOD	$0.231 \pm 2.1 \cdot 10^{-2}$	$9.82 \cdot 10^{-3}$	$9.82 \cdot 10^{-3}$	$1.98 \cdot 10^{9}$	$1.98 \cdot 10^{9}$
bulk $Cu(OH)_2$	$0.384 \pm 2.6 \cdot 10^{-2}$	----	----	----	----

Tab. S3. Change of absorbance at 290 nm due to the formation of uric acid in presence (three different concentrations) and in absence (control) of Gly-$Cu(OH)_2$ NPs. Gly-$Cu(OH)_2$ NPs do not inhibit radical formation in the xanthine/XO system. The effect of Gly-$Cu(OH)_2$ NPs on superoxide generation with a xanthine/xanthine oxidase (XO)-system was investigated by observing the change of absorbance at 290 nm, based on the formation of uric acid as one of the reaction products. The change of absorbance was detected over a period of one minute.

V(NP) [µL] of a 0.1 $mg \cdot mL^{-1}$ stock solution	Change of absorbance at 290 nm [ΔAbs/s]	Error [Δ(ΔAbs/s)]
0	$2.19 \cdot 10^{-3}$	$4.49 \cdot 10^{-5}$
1	$2.09 \cdot 10^{-3}$	$1.11 \cdot 10^{-4}$
5	$1.96 \cdot 10^{-3}$	$1.78 \cdot 10^{-5}$
10	$2.08 \cdot 10^{-3}$	$7.12 \cdot 10^{-5}$

Rate constant of the INT reduction by superoxide

The rate constant for the reduction of INT by superoxide radicals was calculated as outlined below. The decomposition rate (R) of superoxide due to the reaction with SOD or INT can be described as a function of the rate constant (k) and the concentrations of superoxide and INT/SOD.[5]

$$R_{INT} = k_{INT} \cdot \left[\cdot O_2^-\right] \cdot [INT] \quad (1.1)$$

$$R_{SOD} = k_{SOD} \cdot \left[\cdot O_2^-\right] \cdot [SOD] \quad (1.2)$$

If the reduction of INT is inhibited for 50% both rates of the superoxide dismutation are equal.

$$k_{SOD} \cdot \left[\cdot O_2^-\right] \cdot [SOD] = k_{INT} \cdot \left[\cdot O_2^-\right] \cdot [INT] \quad (1.3)$$

(1.3) leads to

$$k_{INT} = k_{SOD} \cdot \frac{[SOD]}{[INT]} \quad (1.4)$$

with $k_{SOD} = 2 \cdot 10^9$ $M^{-1}s^{-1}$.[5] The resulting rate constant of the INT reduction by superoxide is:

$$k_{INT} = 3.94 \cdot 10^4 \ M^{-1}s^{-1} \quad (1.5)$$

Calculation of SOD activities

The calculation of catalytic activities of nanoparticle samples were done in two different ways. While it is widespread to calculate catalytic activities of NPs normalized to a single nanoparticle, we eventually determined the activity *per* active site.

Calculation of IC_{50} value for molar nanoparticle concentrations

IC_{50} values for molar NP concentrations were obtained as outlined below. The number of NPs *per* liter was confirmed using average particle dimensions deduced from TEM and the density of $Cu(OH)_2$. A normalization with the Avogadro constant leads to molar NP concentrations. We approximated the NP morphologies as ideal spheres.

The concentration to achieve a 50% inhibition of the INT reduction was $8.48 \cdot 10^{-5}$ $g \cdot L^{-1}$.

The dimensions of the NPs were obtained from TEM (d = 152.6 nm) and the density of copper(II) hydroxide was used ($\rho_{Cu(OH)2} = 3.368$ $g \cdot cm^{-3}$).

Volume *per* particle (V_{NP}):

$$V_{NP} = = 1.86 \cdot 10^{-15} \ cm^3 \quad (1.6)$$

Mass *per* nanoparticle ($m_{NP)}$:

$$m_{Np} = \rho_{Cu(OH)2} \cdot V_{NP} = 6.27 \cdot 10^{-15} \ g = 6.27 \cdot 10^{-9} \ \mu g \quad (1.7)$$

With the measured amount of Gly-$Cu(OH)_2$-NPs to achieve a 50% inhibition of the INT reduction and the amount of copper hydroxide (84%) determined by AAS, an IC_{50} concentration of $IC_{50} = 8.48 \cdot 10^{-5}$ $g \cdot L^{-1}$ was calculated. The molar nanoparticle concentration was determined with Avogadro´s constant.

$$(NPs \cdot L^{-1}) = IC_{50} \cdot m_{Np}^{-1} = 1.35 \cdot 10^{10} \ L^{-1} \quad (1.8)$$

$$c_{NP} = (NP \cdot L^{-1}) \cdot N_A^{-1} = 2.25 \cdot 10^{-14} \ \mu M \quad (1.9)$$

Calculation of SOD activity per active site

The catalytic activity of Gly-$Cu(OH)_2$-NPs was calculated normalized to an active surface site. For nanomaterials, as only surface atoms (Figure S4, red) are involved in catalytic reactions, while Cu atoms in the bulk (Figure S4, green) are not accessible to surface reactions and therefore inactive.

Figure S4 illustrates the approach to estimate the number of catalytically active surface atoms with respect to the number of bulk atoms per nanoparticle from the particle volume and the bulk analytical composition.

With the average NP diameter (d=152.6 nm) the average surface area (SA_{NP}) and the average volume (V_{NP}) of a single NP were determined. For simplicity, the NPs were approximated as ideal spheres.

$$\text{Surface area: } SA_{NP} = \pi d^2 = 7.32 \cdot 10^4 \text{ nm}^2 \quad (1.10)$$

$$\text{Volume: } V_{NP} = (1/6)\,\pi d^3 = 1.86 \cdot 10^6 \text{ nm}^3 \quad (1.11)$$

The number of active sites *per* NP was estimated based on the $Cu(OH)_2$ crystal structure (lepidocrocyte type) assuming that the particles are terminated by the [310] surface. The unit cell parameters are a = 0.0294741 nm; b = 0.10593 nm; c = 0.052564 nm (determined by P-XRD, Table S1).

The surface area of the terminating [310] layer was determined from the unit cell parameters.

$$\text{Surface area of terminating surface: } SA_{[310]} = 5.59 \cdot 10^{-3} \text{ nm}^2 \quad (1.12)$$

$$\text{Volume unit cell: } V_{UC} = a \cdot b \cdot c = 1.64 \cdot 10^{-4} \text{ nm}^3 \quad (1.13)$$

The unit cell contains four Cu atoms in total, two Cu atoms are situated at the [310] surface layer. The number of [310] layers at the NP surface is given as quotient of the surface area (SA) of a NP and the surface area of the terminating layer:

$$N_{[310]} = SA_{NP} / SA_{[310]} = 1.31 \cdot 10^7 \quad (1.14)$$

The number of catalytic active Cu atoms per unit cell is equal to the number of Cu atoms on the [310] layer:

$$N_{\text{catalytic active Cu atoms}} = N_{\text{Atoms at [310]}} \cdot N_{[310]} = 2.62 \cdot 10^7 \quad (1.15)$$

In an analogue way the amount of unit cells *per* nanoparticle ($N_{UC/NP}$) was determined as quotient of the nanoparticle volume and the unit cell volume:

$$N_{UC/NP} = V_{NP} \cdot V_{UC}^{-1} = 1.13 \cdot 10^{10} \quad (1.16)$$

The number of Cu atoms *per* nanoparticle ($N_{Cu/NP}$) is obtained by multiplication with the number of Cu atoms *per* unit cell (4):

$$N_{Cu/NP} = N_{Cu/UC} \cdot N_{UC} = 4.53 \cdot 10^{10} \quad (1.17)$$

The ratio of (catalytically active) Cu surface and (inactive) bulk atoms were used to calculate the total concentration of active Cu(II) sites from the total Cu concentration (determined by AAS).

$$P = (N_{\text{catalytic active Cu atoms}]}) \cdot (N_{Cu/NP})^{-1} = 5.78 \cdot 10^{-4} \quad (1.18)$$

Rate constants of the SOD reaction catalyzed by Gly-$Cu(OH)_2$ NPs

Rate constants were determined using equation (1.19) and $k_{INT} = 3.94 \cdot 10^4$ $M^{-1}s^{-1}$ (1.5).

$$k_{Cu(OH)2} = k_{INT} \cdot \frac{[INT]}{[Cu(OH)_2]} \quad (1.19)$$

References

1. Sen, D. N.; Mizushima, S.-I.; Curran, C.; Quagliano, J. V. *J. Am. Chem. Soc.* 1955, **77**, 211–212.
2. O'Brien, P. *J. Chem. Educ.* 1982, **59**, 1052–1053.
3. Evans, D. F. *J. Chem. Soc.* 1959, 2003–2005.
4. J. Strozynski, J. Heim, S. Bunbanjerdsuk, N. Wiesmann, J. Zografidou, S. K. Becker, A. M. Meierl, H. Gouveris, H. Lüddens, F. Grus, J. Brieger, *J. Proteomics* 2015, **113**, 154–161.
5. McCord, J. M. *Curr. Protoc. Toxicol.* 2001, Chapter **7**, Unit 7.3.